at room temperature in bicarbonate-buffered Ames medium, and fluorescent-labeled cells were identified as described (*35*). Detachment from pigment epithelium and exposure to bright light during dissection (~1×10^{17} photons s^{-1} cm^{-2} measured at 500 nm) and epifluorescence examination (~3×10^{17} photons s^{-1} cm^{-2} at 560 nm) presumably strongly bleached rod and cone photopigments. Ganglion cell somata were exposed by microdissection. Whole-cell current clamp recordings were made with an intracellular amplifier (Cygnus Technologies DR-886, Delaware Water Gap, PA) and micropipettes (3 to 7 megaohms) containing 125 mM K-Gluconate, 5 mM NaCl, 4 mM KCl, 10 mM EGTA, 10 mM Hepes, 4 mM adenosine triphosphate–Mg, 7 mM phosphocreatine, 0.3 mM guanosine triphosphate–tris, LY (0.1% w/v), and biocytin (0.5% w/v). Resting potentials were not corrected for liquid junction potentials. Light stimuli were introduced from below with the microscope's 100-W tungsten-halogen lamp and transillumination optics. Neutral density and narrow-band interference filters (Oriel, Stratford, CT) controlled stimulus energy and wavelength. Energies were measured with a calibrated radiometer (UDT Instruments, Baltimore, MD). Except where noted, all stimuli were full-field and spectrally unfiltered.

11. The probability of obtaining such light responses was very high among back-filled cells in very sparsely labeled retinas but declined substantially when labeled ganglion cells totaled >100, presumably because involvement of the chiasm reduced labeling specificity. Peak depolarizations for saturating stimuli typically ranged from 15 to 30 mV.
12. Cobalt chloride was superfused at a concentration (2 mM in Ames) that blocks all light-evoked transmitter release from rods and cones in rat retina (*36*) and eliminates the otherwise robust light responses of ganglion cells in rat and cat eyecup preparations (*37*). Small chamber volume (<200 μl) and inlet tubing dead space (<2 ml) ensured complete exchange in minutes. Light responses also persisted when 2 mM $[Co^{2+}]_o$ replaced 2 mM $[Ca^{2+}]_o$ in a bath solution containing 126 mM NaCl, 3 mM KCl, 1.3 mM NaH_2PO_4, 2 mM $MgSO_4$, 26 mM $NaHCO_3$, and 10 mM dextrose (n = 2).
13. In darkness, resting potentials of photosensitive (−46.7 ± 14.8 mV; n = 114) and control ganglion cells (−48.5 ± 11.0 mV; n = 45) were statistically indistinguishable ($P > 0.2$; t test).
14. For most cells (n = 4; including that shown in Fig. 1G), the drug solution consisted of 2 mM $CoCl_2$, 100 μM L(+)-2-amino-4-phosphonobutyric acid to saturate and thus block signal transfer at Group III metabotropic glutamate receptors essential for photoreceptor-to-ON-bipolar cell transmission, 20 μM 6,7-dinitroquinoxaline-2,3-dione and 50 μM DL-2-amino-5-phosphonovaleric acid to block ionotropic glutamate receptors [both *N*-methyl-D-aspartate (NMDA) and non-NMDA types] essential for communication between photoreceptors and OFF bipolar cells and between all bipolar cells and both amacrine and ganglion cells, and 50 μM picrotoxin and 0.3 μM strychnine to block ionotropic gamma-aminobutyric acid (GABA) and glycine receptors mediating most inhibition by amacrine cells. In two other cells, this cocktail was supplemented with 200 μM hexamethonium bromide to block nicotinic acetylcholine receptors and either 500 or 2000 μM 1-octanol to block gap junctions; light-evoked depolarizations were not attenuated. Blockade typically enhanced depolarization (e.g., Fig. 1, F and G; mean depolarization = 18.5 mV in control medium and 26.7 mV during blockade; n = 7). This may reflect increased membrane resistance due to loss of synaptic currents or of intrinsic calcium conductances. Resting potential was not significantly altered by synaptic blockade (means = 52.8 mV in Ames and 51.5 mV during blockade; n = 7).
15. Sensitivity usually deteriorated noticeably within 30 to 120 min of break-in, probably because of cell dialysis ("run-down"). Group data in Fig. 2C (green curve) were therefore drawn only from responses obtained shortly after break-in, first at 500 nm and then at one other wavelength. Slow recovery kinetics necessitated long interstimulus intervals (3 min). Thus, spectra for single cells were typically less complete than that shown for cell 62-4 (Fig. 2C, red curve). Nonetheless, the general form of the action spectrum was consistent. For example, among each of seven cells examined, the same rank order of sensitivity applied to the first three wavelengths tested: 500 nm > 400 or 420 nm ≫ 570 or 600 nm.

16. J. S. Takahashi, P. J. DeCoursey, L. Bauman, M. Menaker, *Nature* **308**, 186 (1984).
17. I. Provencio, R. G. Foster, *Brain. Res.* **694**, 183 (1995).
18. Differences between these physiological and behavioral curves may be attributable in part to spectral filtering by the lens, which presumably influenced the behavioral spectrum but not the data we obtained in isolated retina. Available spectral data do not exclude contributions of rods or green cones to the entrainment mechanism (*17*, *26*).
19. L. Barr, M. Alpern, *J. Gen. Physiol.* **46**, 1249 (1963).
20. A. Daniolos, A. B. Lerner, M. R. Lerner, *Pigment Cell Res.* **3**, 38 (1990).
21. D. S. Hsu *et al.*, *Biochemistry* **35**, 13871 (1996).
22. Values are based on a 2-mm pupil and retinal area of 1.13 cm^2 (*38*). For comparison, absolute rod threshold in the rat is ~2×10^{-4} cd/m^2 [(*39*) as cited by (*27*)] or ~ 10^7 photons cm^{-2} s^{-1} retinal irradiance.
23. O. Dkhissi-Benyahya, B. Sicard, H. M. Cooper, *J. Neurosci.* **20**, 7790 (2000).
24. D. E. Nelson, J. S. Takahashi, *Am. J. Physiol.* **277**, R1351 (1999).
25. J. H. Meijer, K. Watanabe, J. Schaap, H. Albus, L. Detari, *J. Neurosci.* **18**, 9078 (1998).
26. N. C. Aggelopoulos, H. Meissl, *J. Physiol.* **523** (part 1), 211 (2000).
27. D. E. Nelson, J. S. Takahashi, *J. Physiol.* **439**, 115 (1991).
28. Immunostaining for LY, avidin-biotin-peroxidase reaction, and diaminobenzidine histochemistry were as described (*35*).
29. M. Pu, *J. Comp. Neurol.* **414**, 267 (1999).
30. ———, *J. Biol. Rhythms* **15**, 31 (2000).
31. Receptive fields were probed with spots or bars generated by placing an aperture in the microscope's spectrally unfiltered transilluminating tungsten beam and focusing it on the tissue with a ×20 objective lens. There was substantial spatial summation within the receptive field, but no surround antagonism, an otherwise ubiquitous feature of ganglion cell receptive fields.
32. S. Hattar, H.-W. Liao, M. Takao, D. M. Berson, K.-W. Yau, *Science* **295**, 1065 (2002).
33. J. J. Gooley, J. Lu, T. C. Chou, T. E. Scammell, C. B. Saper, *Nature Neurosci.* **4**, 1165 (2001).
34. J. Hannibal, P. Hindersson, S. M. Knudsen, B. Georg, J. Fahrenkrug, *J. Neurosci.* **22**, RC191 (2002).
35. M. Pu, D. M. Berson, *J. Neurosci. Methods* **41**, 45 (1992).
36. D. G. Green, N. V. Kapousta-Bruneau, *Vis. Neurosci.* **16**, 727 (1999).
37. F. A. Dunn, B. J. O'Brien, unpublished data.
38. A. Hughes, *Vision Res.* **19**, 569 (1979).
39. E. Dodt, K. Echte, *J. Neurophysiol.* **24**, 427 (1961).
40. D. M. Berson, F. A. Dunn, M. Takao, data not shown.
41. T. D. Lamb, *Vision Res.* **35**, 3083 (1995).

42. We thank B. Wooten for assistance with the spectral analysis; M. Seibert for help with the receptive field study; T. Nguyen for technical assistance; and H. Wässle, B. O'Brien, J. McIlwain, I. Provencio, M. Slaughter, and L. Peichl for their valuable comments on the manuscript. Supported by NIH grant EY12793 to D.M.B.

18 October 2001; accepted 7 January 2002

Metabolic Enzymes of Mycobacteria Linked to Antioxidant Defense by a Thioredoxin-Like Protein

R. Bryk,[1,4]* C. D. Lima,[2,5]* H. Erdjument-Bromage,[3] P. Tempst,[3,5,6] C. Nathan[1,4,6]†

Mycobacterium tuberculosis **(Mtb) mounts a stubborn defense against oxidative and nitrosative components of the immune response. Dihydrolipoamide dehydrogenase (Lpd) and dihydrolipoamide succinyltransferase (SucB) are components of α-ketoacid dehydrogenase complexes that are central to intermediary metabolism. We find that Lpd and SucB support Mtb's antioxidant defense. The peroxiredoxin alkyl hydroperoxide reductase (AhpC) is linked to Lpd and SucB by an adaptor protein, AhpD. The 2.0 angstrom AhpD crystal structure reveals a thioredoxin-like active site that is responsive to lipoamide. We propose that Lpd, SucB (the only lipoyl protein detected in Mtb), AhpD, and AhpC together constitute a nicotinamide adenine dinucleotide (reduced)–dependent peroxidase and peroxynitrite reductase. AhpD thus represents a class of thioredoxin-like molecules that enables an antioxidant defense.**

Mtb, the leading cause of death from a single bacterial species, is restrained from proliferation in most infected individuals by oxidative and nitrosative stress imposed in part by inducible nitric oxide synthase (*1*, *2*). Yet despite the immune response, viable mycobacteria persist. Bacterial persistence has directed our attention to Mtb's defenses against oxidative and nitrosative stress.

Mtb peroxiredoxin alkyl hydroperoxide reductase (AhpC), a member of the peroxiredoxin family of nonheme peroxidases, protects heterologous bacterial and human cells against oxidative and nitrosative injury (*3*, *4*). The redundancy of peroxiredoxins in Mtb complicates interpretation of the phenotype of an *ahpC*-deficient mutant (*5*). AhpC metabolizes peroxides (*6*) and peroxynitrite (*7*) via a conserved

NH_2-terminal cysteine residue, which undergoes oxidation. To complete the catalytic cycle, the Cys residue must be reduced. Various peroxiredoxins rely on diverse reducing systems, including AhpF; thioredoxin and thioredoxin reductase; tryparedoxin, trypanothione, and trypanothione reductase; and cyclophilin (*8*). It is not known what serves as an AhpC reductase in Mtb. The genome of Mtb H37Rv encodes no AhpF-like proteins (*9*). Mtb thioredoxin reductase and thioredoxin did not support the peroxidase activity of AhpC (*10*). The Mtb *ahpC* gene lies 11 nucleotides upstream of a coding region denoted *ahpD*, based on its sharing a bicistronic operon with *ahpC*. Recombinant AhpD functioned as a weak peroxidase but did not appear to interact with AhpC physically or functionally (*10*).

To search for an AhpC reductase in Mtb, we investigated whether pure AhpC (*7*) could reduce H_2O_2 when supplemented with lysate (*11*) from Mtb H37Rv. Neither nicotinamide adenine dinucleotide, reduced (NADH) nor nicotinamide adenine dinucleotide phosphate, reduced (NADPH) supported peroxidase activity by AhpC in the presence of lysate (Fig. 1A). However, the addition of pure AhpD (*11*) produced a robust, NADH-dependent, cyanide-insensitive peroxidase activity. Single mutants with a cysteine to serine substitution (AhpD C130S; AhpD C133S) (*11*) could not replace wild-type AhpD. AhpD by itself showed minimal peroxidatic activity, as reported (*10*) (*12*). On the scale of the reaction in Fig. 1A, the contribution of AhpD alone was imperceptible.

We purified an activity from Mtb lysate that sustained AhpD-dependent peroxidase activity of AhpC through fractional ammonium sulfate precipitation and anion exchange. Further purification led to complete loss of activity, suggesting that there were two separable components. We therefore compared the activity profile of fractions from Q Sepharose with the corresponding Coomassie blue–stained protein banding pattern. The abundance of three polypeptide bands most closely matched the peak activity (Fig. 1B). As revealed by peptide mass fingerprinting (*13*, *14*), two of the three bands corresponded to hypothetical protein Rv0462 [National Center for Biotechnology Information (NCBI) accession number 7431875], Mtb's sole dihydrolipoamide dehydrogenase (Lpd) (*15*). The identification was based on eight tryptic matches with an average difference of 0.006 absolute mass units (amu) between observed and predicted masses, covering 30% of the coding sequence.

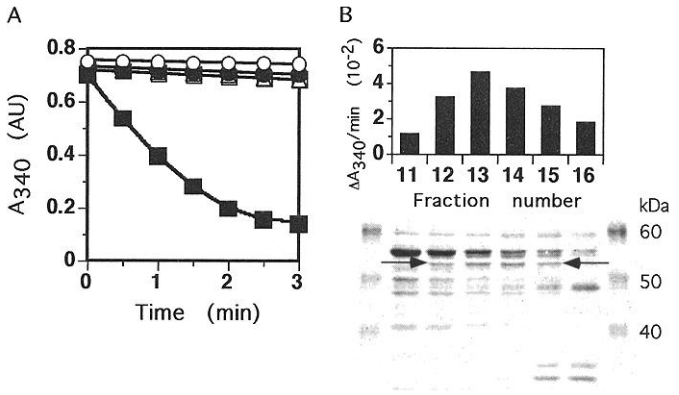

Fig. 1. Identification of Lpd (Rv0462) as a component of the AhpC/AhpD–dependent peroxidase system. **(A)** Mycobacterial lysates support AhpC peroxidase activity only in the presence of AhpD. Reaction mixtures (0.5 ml) contained 30 mM potassium phosphate (KPi) at pH 7.0, 0.625 mM EDTA, 125 μM NADH, 5 μM recombinant AhpC, 10 μM recombinant AhpD, and 50 μl (3.8 mg/ml) *Mtb* H37Rv lysate (solid squares). Reactions were initiated by the addition of 0.5 mM H_2O_2, and consumption of NADH was determined by measuring the absorbance at 340 nm (A_{340}). Control reactions were carried out with no AhpC (open squares), no AhpD (open triangles), no lysates (open circles), or 125 μM NADPH (solid circles) instead of NADH. **(B)** Elution profile from Q Sepharose. The bar diagram shows the peak activity profile of fractions tested as in (A), with the corresponding Coomassie-stained SDS–10% polyacrylamide gel electrophoresis (SDS-PAGE) displayed below. Arrows point to the protein band used for peptide mass fingerprinting.

Lpd is a flavin-adenine dinucleotide–containing NADH-dependent oxidoreductase that plays an essential role in intermediary metabolism as the E3 component of pyruvate dehydrogenase (PDH), α-ketoglutarate dehydrogenase (KGDH), and branched-chain α-keto acid dehydrogenase (BCKADH) complexes (*16*). In these complexes, Lpd regenerates the dihydrolipoic (6,8-dithiooctanoic acid) acceptors covalently attached to ε-amino groups of lysine residues on the "swinging arm(s)" of the E2 acetyl(succinyl-)transferase component (*16*). To confirm that Lpd could replace mycobacterial lysate, we added bovine Lpd (0.2 U) to AhpC + AhpD + NADH. H_2O_2-dependent consumption of NADH ensued, but only when we further supplemented the reaction with 50 μM lipoamide (the amide of 6,8-dithiooctanoic acid) (*11*). Lpd by itself, with or without lipoamide, sustained only 10 to 15% of the peroxidase activity of AhpC + AhpD + Lpd + lipoamide.

We reasoned that knowing the structure of AhpD might help us understand how AhpD interacts with Lpd and lipoamide in sustaining the peroxidase activity of AhpC. We crystallized AhpD and solved its structure at 2.0 Å resolution by x-ray diffraction (*11*). AhpD proved to be a trimer. The AhpD protomer is nearly all helical except for residues 93 to 113, which adopt an extended conformation between protomer contacts (Fig. 2A). Trimerization is sustained by interactions between helices α2, α8, α6, and α7 from one protomer and helix α5 and residues 96 to 104 from an adjacent protomer. The protomers interact via hydrophobic contacts, hydrogen bonds, and salt bridges. No structural homology was revealed when protomer or trimer models were used in searches with the programs DALI or PFAM (*17*). Because the AhpD cysteines were critical for activity, we tried to align them with the active site of the thioredoxin family. Thioredoxins share the Cys-X-X-Cys signature but no other amino acid sequence homology with AhpD. Structure-based alignment revealed that the AhpD fold's active site (one per protomer) at the NH_2-terminus of helix α7 is structurally similar to that of thioredoxins, as illustrated for thioredoxins from *Escherichia coli* and T4 bacteriophage (Fig. 2B). The AhpD structure was solved in reduced form, in which the sulfhydryls of the two active-site cysteines lie 3.5 Å apart. To test if these two Cys could undergo disulfide bonding, we resolved the structure of AhpD after oxidation by lipoamide. This brought the AhpD sulfhydryls to within 2.0 to 2.1 Å (Fig. 2, B and C), the same distance as in oxidized thioredoxin (Fig. 2B). In contrast, after exposure to H_2O_2, the intersulfhydryl distance was indeterminate, which suggested that only a fraction of the AhpD molecules were oxidized and that lipoamide was a better oxidant of AhpD than H_2O_2 (*12*). After oxidation, the trimer remained intact. Oxidation induced no other changes aside from minor compensatory movements in the position of helix α7 (Fig. 2C) and rotation of the imidazole of His^{132} away from Cys^{133} (*12*).

Cys^{133} lies at the base of the active-site cleft, where it is accessible to interactions with large molecules (*11*). Cys^{130} is partially buried within the fold and appears to be blocked from potential ligand interactions by protomer-protomer contacts. Each protomer's active-site cleft is lined almost entirely by polar and hydrophobic side chains. This suggested that each of the three active sites in the trimer could be accessed by a redox-active moiety offered via a hydrophobic structure, such as lipoamide. Each protomer's cleft is also large enough to serve as a potential ligand-binding pocket for AhpC (*11*).

[1]Department of Microbiology and Immunology, [2]Department of Biochemistry, Weill Medical College of Cornell University, New York, NY 10021, USA. [3]Protein Center, Sloan-Kettering Institute, New York, NY 10021, USA. [4]Program in Immunology, [5]Program in Structural Biology, [6]Program in Molecular Biology, Weill Graduate School of Medical Sciences of Cornell University, New York, NY 10021, USA.

*These authors contributed equally to this work.
†To whom correspondence should be addressed at Box 65, Weill Medical College, 1300 York Avenue, New York, NY 10021, USA. E-mail: cnathan@med.cornell.edu

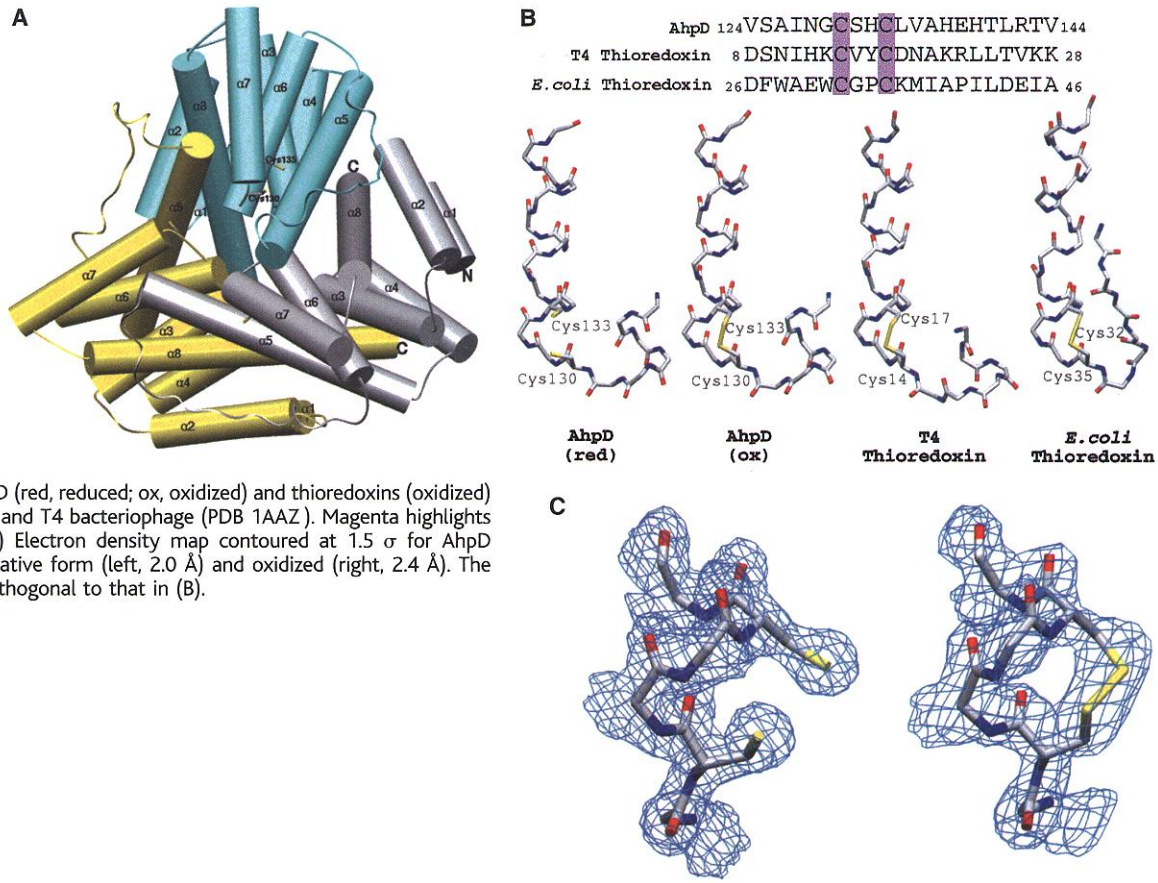

Fig. 2. AhpD crystal structure. (**A**) Architecture of the AhpD trimer (reduced form). Helices are denoted by tubes designated α (numbered from NH_2- to COOH-terminus), and connecting peptides are designated by ribbons. Monomers are blue, yellow, and gray. Cys^{130} and Cys^{133} are best seen on α7 of the blue protomer. The graphics were prepared with SETOR (*26*). (**B**) Structure-based least-squares sequence alignment between active-site cysteines and helices in AhpD (red, reduced; ox, oxidized) and thioredoxins (oxidized) from *E. coli* (PDB 2TRX) and T4 bacteriophage (PDB 1AAZ). Magenta highlights the dicysteine motif. (**C**) Electron density map contoured at 1.5 σ for AhpD active-site cysteines in native form (left, 2.0 Å) and oxidized (right, 2.4 Å). The view is approximately orthogonal to that in (B).

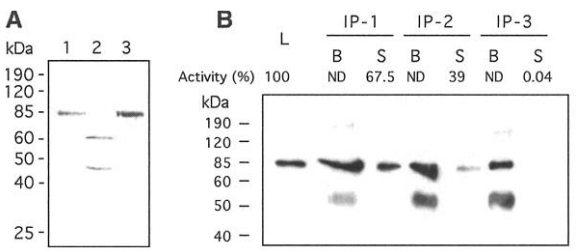

Fig. 3. Identification of SucB (Rv2215) as a component of the AhpC/AhpD–dependent peroxidase system. (**A**) Identification of lipoylated proteins in mycobacterial lysates. Samples were run on an SDS—10% polyacrylamide gel, transferred to nitrocellulose, and subjected to Western blotting with anti–lipoic acid (1:10,000). Lane 1, *M. tb* H37Rv lysate; lane 2, *M. bovis* BCG lysate; lane 3, active peak after Q Sepharose. (**B**) *M. tb* H37Rv lysates depleted of the single lipoylated protein no longer support AhpC peroxidatic activity. Lysates (1.5 mg of total protein) were incubated with anti–lipoic acid (1:200) overnight at 4°C, and immune complexes were precipitated with protein G agarose. Beads were washed three times in 0.5 ml of 50 mM KPi (pH 7.0), 1 mM EDTA, 150 mM NaCl, 10% glycerol, and 0.1% Tween-20 and were boiled with 25 μl of sample buffer. Samples were analyzed by 10% SDS–polyacrylamide gel electrophoresis and visualized by Western blotting with the same antibody (1:5000). L, lysates (50 μg); B, immune complexes on beads (12.5 μl); S, supernatants (50 μg) after the beads were removed. Supernatants (50 μl) were tested for residual activity as in Fig. 1A. Results are expressed as a percentage of starting activity in lysates (100%). Three cycles of IPs (IP-1, IP-2, and IP-3) led to complete depletion. The immunoreactive band at 50 kD corresponds to immunoglobulin G.

In sum, the structural findings suggested that AhpD might function as a specialized form of thioredoxin. We tested the possibility that AhpD mediates electron transfer from a lipoamide moiety to AhpC through reversible disulfide bond formation. We had previously determined that free lipoamide sustained the peroxidase activity of AhpC + AhpD + bovine Lpd and that lipoamide can participate in disulfide exchange with AhpD. However, there is no free lipoamide in cells, and almost all lipoic acid is protein-bound via amide linkage. Thus, we suspected that mycobacterial lysate also supplied a lipoylated protein when it complemented the peroxidase activity of AhpC + AhpD. Indeed, immunoblots of Mtb lysate with an antibody to lipoic acid (anti–lipoic acid) (Fig. 3A) revealed a single lipoylated polypeptide, p85. This species was enriched in the active peak from Q Sepharose (Fig. 3A). For comparison, we studied lysates of another mycobacterial species, *Mycobacterium bovis* BCG (bacillus Calmette-Guérin). BCG lysate was not able to complement AhpC peroxidase activity in the presence of AhpD (*12*) and contained lipolylated species migrating at 46 and 60 kD rather than at 85 kD (Fig. 3A). The p46 and p60 BCG proteins may represent degradation products of p85 or a different set of lipoylated proteins. Nonetheless, the presence of p85 correlated with peroxidase activity.

To test whether the lipoylated protein detected by anti–lipoic acid contributed to peroxidase activity, we used the same antibody to immunodeplete the protein from Mtb lysate. Immunodepletion was carried out in stages to establish a concentration-response relation. Gradual depletion of p85 led to a corresponding and eventually complete loss of the ability of the lysate to support H_2O_2-dependent AhpC activity in the presence of AhpD (Fig. 3B).

Peptide mass fingerprinting identified p85 as a homolog of dihydrolipoamide succinyltransferase, the E2 component of KGDH (Rv2215; NCBI accession number 1709443). This identification was based on 15 tryptic matches with an average difference of 0.036 amu between observed and predicted masses, covering 35% of the coding sequence. A BLAST search of the Mtb H37Rv genome with a consensus lipoylation sequence identified a gene annotated as *sucB* encoding the same protein (*9*). The *sucB* gene encodes two lipoylation

consensus sequences, DEPLVEVST**DKV**D-TEIPSP (*18*), suggesting that SucB is most likely lipoylated at Lys^{43} and Lys^{162}.

To reconstitute peroxidase activity solely with mycobacterial proteins, we cloned Lpd and SucB from Mtb H37Rv, overexpressed the recombinant proteins in *E. coli*, and purified them to homogeneity (*11*). Lpd, SucB, AhpD, and AhpC together sustained H_2O_2-dependent oxidation of NADH (Fig. 4A). No activity was observed when Lpd, AhpD, or AhpC was omitted, nor when Lpd, SucB, AhpD, and AhpC were tested alone or in pairs. In the absence of SucB, the reaction supported by the combination of AhpC + AhpD + Lpd was about 30% of the rate observed in the presence of SucB. The complete system sustained slightly higher levels of activity when cumene and tert-butyl hydroperoxides were substrates in place of H_2O_2 (*12*). At a molar excess of Lpd, SucB, and AhpD, AhpC metabolized H_2O_2 with a catalytic constant (k_{cat}) of 80 min^{-1}, a rate much higher than previously reported for AhpD or AhpC alone (*10*). Further, AhpD catalyzed reversible disulfide exchange with the aromatic dithiol dithionitrobenzene (DTNB) when provided with electrons from NADH via Lpd + SucB (Fig. 4B). DTNB reductase activity was lost when AhpD Cys^{133} was replaced with Ser (Fig. 4B). Lpd and SucB alone sustained less than 7% of the DTNB reductase activity observed in the presence of AhpD (Fig. 4B).

Thus, AhpC, AhpD, SucB, and Lpd together constitute a peroxidase active toward both hydrogen and alkyl peroxides. Considering the relationship that exists between Lpd and SucB, the structural evidence that lipoamide is able to oxidize the AhpD cysteine pair (Fig. 2C), the DTNB reductase activity of LpD + SucB + AhpD (Fig. 4B), and the far greater reactivity of AhpC (*7*) compared with AhpD (*10*) toward peroxides, the sequence of electron flow appears to be NADH → Lpd → SucB → AhpD → AhpC → ROOH. This is opposite to the direction of electron flow when SucB and Lpd participate in α-ketoacid dehydrogenase complexes (Fig. 4C).

We next examined whether the endogenous four-component peroxidase from Mtb could serve as a peroxynitrite reductase. Peroxynitrite was infused into a reaction mixture containing pure recombinant Lpd, SucB, AhpD, AhpC, and NADH (Fig. 4D). The system efficiently metabolized peroxynitrite as assessed by protection of dihydrorhodamine from oxidation. Peroxynitrite reductase activity under these conditions continued for 3 min, after which NADH was depleted. Given the rate of reaction of Mtb AhpC with peroxynitrite (1.33×10^6 $M^{-1}s^{-1}$) (*7*) and the 20-fold molar excess of peroxynitrite over AhpC in this experiment, sustained protection of dihydrorhodamine clearly reflected a catalytic cycle. Under the same conditions, the heterologous system of Mtb AhpC with AhpF from *Salmonella typhimurium* afforded much weaker protection (Fig. 4D). Thus, AhpC + AhpD + SucB + Lpd constitute an endogenous mycobacterial peroxynitrite reductase.

These findings ascribe new functions to three proteins. Each appears to be singular in Mtb, and one or more may hold interest as a drug target for tuberculosis. The structure of AhpD does not resemble any structure previously reported. All other proteins in the thioredoxin superfamily (thioredoxins, glutaredoxins, tryparedoxin, and the Dsb family) share a common fold composed of a four-stranded β sheet and three flanking α helices (*19*). AhpD shares only the COOH-terminal signature motif, Cys-X-X-Cys, disposed as in thioredoxin but within a previously undescribed fold. AhpD homologs have been identified only in mycobacteria, *Streptomycetes*, and a few proteobacteria such as *Bradyrhizobium* and *Caulobacter*.

The Lpd of Mtb (Rv0462) lies in a presumptive operon with several unannotated hypothetical proteins. The only previously demonstrated function of Lpd was as the E3 component of PDH, KGDH, and BCKADH complexes. However, homologs of Lpd are more widely distributed than are the dehydrogenase complexes themselves, occurring in the absence of other components in some anaerobes, archaebacteria, and trypanosomatids (*16*, *20*). This distribution suggests the evolutionary conservation of a previously undescribed function of Lpd. We hypothesize that Lpd may constitute part of a peroxiredoxin-based peroxidase-peroxynitrite

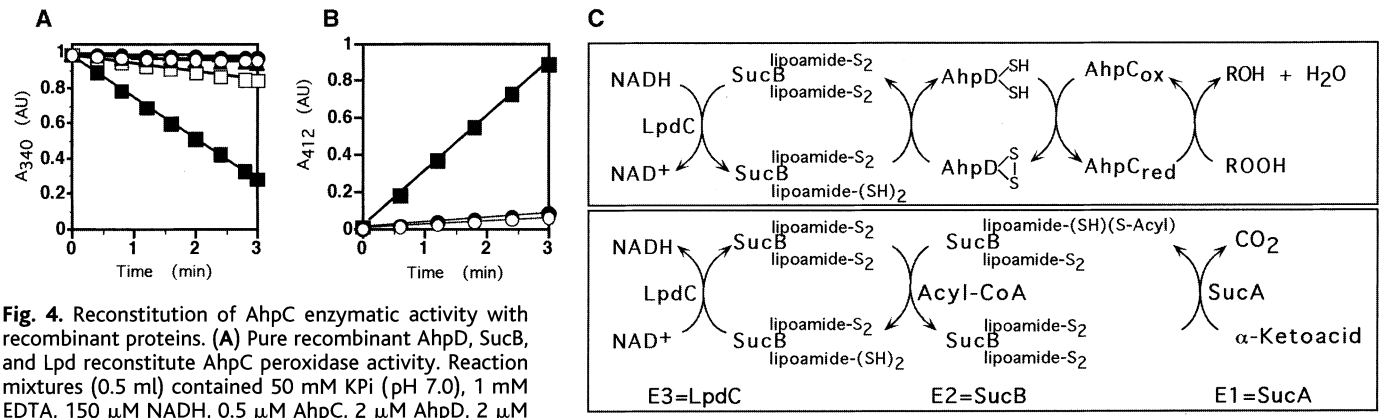

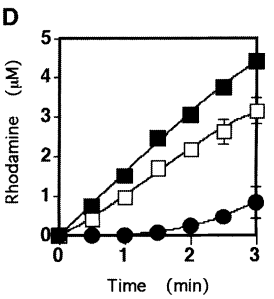

Fig. 4. Reconstitution of AhpC enzymatic activity with recombinant proteins. (**A**) Pure recombinant AhpD, SucB, and Lpd reconstitute AhpC peroxidase activity. Reaction mixtures (0.5 ml) contained 50 mM KPi (pH 7.0), 1 mM EDTA, 150 μM NADH, 0.5 μM AhpC, 2 μM AhpD, 2 μM SucB, and 0.5 μM Lpd (solid squares). Reactions were initiated by the addition of 0.5 mM H_2O_2, and consumption of NADH was monitored by A_{340}. Control reactions were carried out with no Lpd (solid circles), no SucB (open squares), no AhpC (solid triangles), or 2 μM AhpD C130S (open circles) instead of AhpD. (**B**) DTNB reductase activity. Reaction mixtures (0.5 ml) contained 80 mM KPi, 1.6 mM EDTA, 80 μM NADH, 80 μM DTNB, 2 μM Lpd, 2 μM SucB, and 0.25 μM AhpD (solid squares). Control reactions were carried out with no AhpD (open circles) and with 2 μM AhpD C133S (solid circles) instead of AhpD. Reactions were initiated by addition of AhpD, and thionitrobenzene formation (extinction coefficient at 412 nm (ε_{412}) = 13,600 $M^{-1}cm^{-1}$) was followed over time by A_{412}. (**C**) Schematic of electron flow in the four-component peroxidase from NADH to peroxide (top) as compared to an α-ketoglutarate dehydrogenase complex from α-ketoacid to NAD^+ (bottom). In the bottom panel acyl-CoA is generated as a product after decarboxylation of the α-ketoacid substrate by E1 and transfer of the acyl moiety via the lipoamide arms of E2 to CoA. Lipoamide arms are regenerated by E3 to complete the cycle and generate NADH. (**D**) Recombinant AhpD, SucB, and Lpd reconstitute AhpC peroxynitrite reductase activity during steady-state infusion of peroxynitrite. Reaction mixtures (1.5 ml) contained 100 mM KPi (pH 7.0); 100 μM diethylenetriamine pentaacetic acid; 100 μM dihydrorhodamine; 50 μM NADH; and either no protein (solid squares), 2 μM AhpC and 5 μM recombinant *S. typhimurium* AhpF (open squares), or 2 μM AhpC, 5 μM AhpD, 5 μM SucB, and 5 μM Lpd (solid circles). Peroxynitrite was infused from a stock solution of 100 μM in 3 mM NaOH at a rate of 200 μl min^{-1} for 3 min. Samples of 50 μl were withdrawn every 30 s, and rhodamine absorbance was measured at 500 nm. The pH of the reaction did not change. Rhodamine formation was calculated by ε_{500} = 78,800 $M^{-1}cm^{-1}$. Results are means ± SD of triplicates.

reductase in organisms other than Mtb, perhaps involving AhpD-equivalents with a thioredoxin-like active site. Others have suggested an antioxidant function for Lpd related to the role of free lipoic acid as an antioxidant (*21*).

Finally, immunochemistry and bioinformatics suggested that SucB appears to be the only lipoylated protein in Mtb H37Rv. If so, then SucB presumably sustains both the PDH and KGDH activities that were detected in Mtb 30 to 40 years ago but were only partially purified (*22*). *E. coli* has organized into operons its genes encoding PDH (*aceE*, *aceF*, and *lpd*) (*23*) and KGDH (*sucA*, *sucB*, *sucC*, and *sucD*) (*24*). No such gene clusters are evident in Mtb. Near *sucB* lie *lipB* (lipoate protein ligase) and *lipA* (lipoate synthase), which may lipoylate SucB. Mtb's *sucA* (E1 homolog of KGDH) is transcribed divergently elsewhere.

If SucB or Lpd could be inhibited in Mtb without affecting their human counterparts, the Krebs cycle in Mtb as well as the bacillus's ability to synthesize acetyl–coenzyme A (CoA) from endogenous precursors could both be vulnerable. Acetyl-CoA is essential for the glyoxylate shunt that helps sustain persistence of Mtb (*25*) and for formation of the fatty acid–rich cell wall, which constitutes both a barrier and target for chemotherapy. This may be the first known instance in which essential metabolic enzymes also engage in antioxidant defenses.

References and Notes

1. J. Chan, J. Flynn, in *Nitric Oxide and Infection*, F. C. Fang, Ed. (Kluwer Academic/Plenum, New York, 1999), pp. 281–310.
2. C. Nathan, M. U. Shiloh, *Proc. Natl. Acad. Sci. U.S.A.* **97**, 8841 (2000).
3. G. Storz *et al.*, *J. Bacteriol.* **171**, 2049 (1989).
4. L. Chen, Q.-w. Xie, C. Nathan, *Mol. Cell* **1**, 795 (1998).
5. B. Springer *et al.*, *Infect. Immun.* **69**, 5967 (2001).
6. H. R. Ellis, L. B. Poole, *Biochemistry* **36**, 13349 (1997).
7. R. Bryk, P. Griffin, C. Nathan, *Nature* **407**, 211 (2000).
8. S. P. Lee *et al.*, *J. Biol. Chem.* **276**, 29826 (2001).
9. S. T. Cole *et al.*, *Nature* **393**, 537 (1998).
10. P. J. Hillas, F. S. del Alba, J. Oyarzabal, A. Wilks, P. R. Ortiz de Montellano, *J. Biol. Chem.* **275**, 18801 (2000).
11. Supplemental material is available on *Science* Online at www.sciencemag.org/cgi/content/full/1067798/DC1.
12. R. Bryk, C. D. Lima, C. Nathan, data not shown.
13. M. Mann, P. Hojrup, P. Roepstorff, *Biol. Mass Spectrom.* **22**, 338 (1993).
14. H. Erjument-Bromage *et al.*, *J. Chromatogr.* **826**, 167 (1998).
15. A. Argyrou, J. S. Blanchard, *Biochemistry* **40**, 11353 (2001).
16. R. N. Perham, *Annu. Rev. Biochem.* **69**, 961 (2000).
17. L. Holm, C. Sanger, *J. Mol. Biol.* **233**, 123 (1993).
18. Single-letter abbreviations for the amino acid residues are as follows: D, Asp; E, Glu; I, Ile; K, Lys; L, Leu; P, Pro; S, Ser; T, Thr; and V, Val.
19. S. K. Katti, D. M. LeMaster, H. Eklund, *J. Mol. Biol.* **212**, 167 (1990).
20. M. J. Danson, *Biochem. Soc. Trans.* **16**, 87 (1988).
21. N. Haramaki, D. Han, G. J. Handelman, H. J. Tritschler, L. Packer, *Free Radical Biol. Med.* **22**, 535 (1997).
22. P. S. Murthy, M. Sirsi, T. Ramakrishnan, *Am. Rev. Respir. Dis.* **108**, 689 (1973).
23. P. E. Stephens, M. G. Darlison, H. M. Lewis, J. R. Guest, *Eur. J. Biochem.* **133**, 481 (1983).
24. M. E. Spencer, M. G. Darlison, P. E. Stephens, I. K. Duckefield, J. R. Guest, *Eur. J. Biochem.* **141**, 361 (1984).
25. J. D. McKinney *et al.*, *Nature* **406**, 735 (2000).
26. S. V. Evans, *J. Mol. Graphics* **11**, 134 (1993).

27. We thank S. Ehrt for mycobacterial lysates, L. Szweda for providing antibodies to lipoic acid, and the staff of beamline X4A at the National Synchrotron Light Source, which is supported by the Howard Hughes Medical Institute. The Department of Microbiology and Immunology acknowledges the support of the William Randolph Hearst Foundation. Supported by a Norman and Rosita Winston fellowship (R.B.), a Young Investigator Award from the Arnold and Mabel Beckman Foundation (C.D.L.), National Cancer Institute Cancer Core Grant P30 CA08748 (P.T.), and NIH grant HL61241 (C.N.). Coordinates and structure factors for AhpD have been deposited with the Protein Data Bank (PDB) with accession number 1KNC.

6 November 2001; accepted 8 January 2002
Published online 17 January 2002;
10.1126/science.1067798
Include this information when citing this paper.

Adult-Onset Primary Open-Angle Glaucoma Caused by Mutations in Optineurin

Tayebeh Rezaie,[1] Anne Child,[2,3] Roger Hitchings,[3] Glen Brice,[2,3] Lauri Miller,[4] Miguel Coca-Prados,[5] Elise Héon,[6] Theodore Krupin,[7] Robert Ritch,[8] Donald Kreutzer,[4] R. Pitts Crick,[9] Mansoor Sarfarazi[1]*

Primary open-angle glaucoma (POAG) affects 33 million individuals worldwide and is a leading cause of blindness. In a study of 54 families with autosomal dominantly inherited adult-onset POAG, we identified the causative gene on chromosome 10p14 and designated it *OPTN* (for "optineurin"). Sequence alterations in *OPTN* were found in 16.7% of families with hereditary POAG, including individuals with normal intraocular pressure. The *OPTN* gene codes for a conserved 66-kilodalton protein of unknown function that has been implicated in the tumor necrosis factor–α signaling pathway and that interacts with diverse proteins including Huntingtin, Ras-associated protein RAB8, and transcription factor IIIA. Optineurin is expressed in trabecular meshwork, nonpigmented ciliary epithelium, retina, and brain, and we speculate that it plays a neuroprotective role.

Glaucoma affects over 67 million people worldwide (*1*) and is the second largest cause of bilateral blindness in the world, after cataracts (*2*). The most common form is POAG, which includes a subgroup termed normal-pressure (NPG) or low-tension glaucoma (LTG) (*3*–*7*). Glaucoma is genetically heterogeneous (*8*). At least eight loci have been linked to the disorder, and two genes have been identified: *CYP1B1*, encoding cytochrome P4501B1 enzyme, is mutated in primary congenital glaucoma (*9*, *10*), and *MYOC*, encoding myocilin, is mutated in juvenile-onset POAG (*11*). Here we identify one of the genes responsible for adult-onset POAG. With approval from the Human Genome Organization (HUGO) nomenclature committee, we designate the gene *OPTN* and its protein product optineurin (for "optic neuropathy inducing" pro-

Table 1. *OPTN* sequence alterations in hereditary adult-onset POAG.

Exon	cDNA change*	Predicted protein change	Number of observed mutations/families (%)	Number of observed mutations/normal chromosomes†	*P* values‡
			Disease-causing alterations		
4	c.458G>A	E50K	7/52 (13.5)	0/540	2.74×10^{-8}
6	c.691_692insAG	Premature stop	1/46 (2.2)	0/200	0.187
16	c.1944G>A	R545Q	1/46 (2.2)	0/100	0.315
	Totals		9/54§ (16.7)	0.0	5.03×10^{-5}‖
			Risk-associated alteration		
5	c.603T>A	M98K	23/169 (13.6)¶	9/422 (2.1)	2.18×10^{-7}

*New nomenclature is used (*22*). Nucleotides are numbered as in GenBank accession number AF420371. †Normal chromosomes were from Caucasian individuals with a similar age group. ‡*P* values for Fisher's exact test. §These 54 glaucoma families were screened by SSCP analysis for the entire of *OPTN*. ‖Only 100 shared chromosomes were used for calculation of this *P* value. ¶Within this group of 169 subjects, M98K was observed in 8 of 45 (17.8%) familial and 15 of 124 (12.1%) sporadic individuals with glaucoma. Most of these individuals have normal IOP and were screened for sequence changes only in exon 5.